Taylor & Francis
Taylor & Francis Group

RESEARCH PAPER

Check for updates

Upstream open reading frames mediate autophagy-related protein translation

Ying Yang [a], Damián Gatica[a], Xu Liu[a], Runliu Wu[b], Rui Kang [b], Daolin Tang [b], and Daniel J. Klionsky [a]

aDepartment of Molecular, Cellular and Developmental Biology, and Life Sciences Institute, University of Michigan, Ann Arbor, MI 48109, USA; bDepartment of Surgery, University of Texas Southwestern Medical Center, Dallas, TX 75390, USA

ABSTRACT
Macroautophagy/autophagy, a highly conserved catabolic pathway that maintains proper cellular homeostasis is stringently regulated by numerous autophagy-related (Atg) proteins. Many studies have investigated autophagy regulation at the transcriptional level; however, relatively little is known about translational control. Here, we report the upstream open reading frame (uORF)-mediated translational control of multiple Atg proteins in *Saccharomyces cerevisiae* and in human cells. The translation of several essential autophagy regulators in yeast, including Atg13, is suppressed by canonical uORFs under nutrient-rich conditions, and is activated during nitrogen-starvation conditions. We also found that the predicted human *ATG4B* and *ATG12* non-canonical uORFs suppress downstream coding sequence translation. These results demonstrate that uORF-mediated translational control is a widely used mechanism among *ATG* genes from yeast to human and suggest a model for how some *ATG* genes bypass the general translational suppression that occurs under stress conditions to maintain a proper level of autophagy.

Abbreviations: 5′ UTR, 5′ untranslated region; Atg, autophagy-related; CDS, coding sequence; Cvt, cytoplasm-to-vacuole targeting; HBSS, Hanks' balanced salt solution; PA, protein A; PE, phosphatidylethanolamine; PIC, preinitiation complex; PtdIns3K, phosphatidylinositol 3-kinase; qRT-PCR, quantitative reverse transcription PCR; Ubl, ubiquitin-like; uORF, upstream open reading frame; WT, wild-type.

Introduction

Macroautophagy (hereafter referred to as autophagy) is an evolutionarily conserved cellular process in which intracellular components and dysfunctional organelles are delivered to lysosomes/vacuoles for degradation and recycling [1]. Aberrant autophagy has been implicated in a series of diseases, including tumorigenesis, neurodegeneration, and metabolic diseases [2,3]. To date, more than 40 autophagy-related (*ATG*) genes has been identified as components of the autophagy pathway in yeast [4]. As a highly conserved process among eukaryotes, most of the protein products of these *ATG* genes have homologs or functional counterparts in human. Under nutrient-rich conditions, autophagy is preserved at a relatively low level to work as a cellular quality control mechanism. Upon stress conditions, such as nutrient deprivation, high-level autophagy is induced to effectively promote bioenergetic homeostasis and maintain cell survival. Active autophagy is largely dependent on proper expression of *ATG* genes. Previous studies have demonstrated many transcriptional activators and repressors in autophagy regulation [5]; however, little is known about how cells efficiently regulate autophagy at the level of translation.

Of note, during stress conditions, such as nutrient limitation, translational activity of most genes is downregulated to save metabolic energy and avoid the generation of dysfunctional proteins. The global translational downregulation of genes upon stress induction is achieved through Sui2/eIF2α

phosphorylation, which affects formation of the 43S preinitiation complex involved in eukaryotic translation initiation [6]. Though cellular stress leads to globally decreased translation of most genes, a small number of mRNAs display upregulated translational activity. For example, many *ATG* genes are reported to bypass the global translational suppression induced by Sui2/eIF2α phosphorylation during nutrient deprivation [7]. Recently, two studies from our lab showed that Dhh1, a DExD/H-box RNA helicase, and Psp2, an RGG motif protein, are engaged in efficient translational regulation of Atg1 and Atg13, two important components of the Atg1 kinase complex, the key autophagy initiator [8,9]. In addition, translation of ATG5, ATG7, ATG12, ATG16L1, and BECN1 are regulated by some RNA-binding proteins such as ELAVL1/HuR and ELAVL4/HuD, HNRNPA1/hnRPA1, and ZFP36/TTP [10–14]. However, it is not clear how other *ATG* genes get upregulated as part of the translational reprogramming that occurs under stress conditions.

Upstream open reading frames (uORFs) are short coding sequences with start codons located in the 5' untranslated region (5' UTR) of eukaryotic mRNAs [15]. Though most translation events occur via the main ORF of mRNAs, many translation events also occur within the 5' UTR of a gene, including those that initiate at uORFs. The stop codon of a uORF is typically located before the stop codon of the protein coding sequence (CDS). Therefore, a uORF may either end before the start of the CDS or may partially overlap

with the CDS depending on the location of its associated stop codon. It is widely accepted that in most cases, uORFs act as important *cis*-regulatory elements to contrtol translation of the corresponding CDS, especially upon amino acid starvation [16]. Nearly half of the mRNA transcripts in yeast and human possess uORFs [15,17]. However, not all uORFs are active in translation regulation, and the mechanism for how uORFs modify CDS translation varies on a case-by-case basis. Currently, proposed models for how uORFs alter CDS translation include leaky scanning, translation reinitiation and ribosome stalling [18–20]. In addition, it is proposed that the peptide produced by a uORF may have biological functions [21]. As uORFs of many genes, such as *GCN4* in yeast and *ATF4* in mammals [19,22], are closely correlated with stress-activated gene upregulation, we raised the question of whether uORFs play a role in downregulating *ATG* gene expression to help maintain a basal level of autophagy under nutrient-rich conditions; bypass of the uORFs would allow increased gene expression when cells are undergoing global translation suppression during stress.

In this paper, we report that uORFs are involved in the translational control of a multitude of *ATG* genes in both *S. cerevisiae* and human cells. We first demonstrate that an *ATG13* uORF acts as a *cis*-acting element, the bypass of which facilitates translational expression of Atg13 in response to stress-induced eIF2 phosphorylation in yeast. The translational event of Atg13 mediated by the uORF is dependent on the surrounding contexts of the uORF start codon, and on the Gcn2 kinase. We also find that at least four uORFs of yeast *ATG5* differentially contribute to *ATG5* translational control; bypass of the *ATG5* and *ATG13* uORFs results in increased autophagy activity. Yeast *ATG12* and yeast *ATG19* possess at least one active uORF, to regulate downstream CDS translation. In addition to the aforementioned *ATG* genes in yeast, a series of genes encoding the core autophagy machinery with potential active uORFs in human cells are delineated here. We determine that the predicted active non-canonical uORFs of *ATG4B* and *ATG12* strongly impede CDS translation in human cells. Altogether, our results show that uORFs have a widespread impact on translational control of *ATG* genes to mediate stress-induced autophagy.

Results

An inhibitory ATG13 *uORF mediates Atg13 expression in response to nitrogen starvation*

Ribosome profiling, also known as Ribo-seq, utilizes high-throughput sequencing to identify short mRNA fragments that are protected by 80S ribosomes, and therefore provides extensive information on the translational events governed by the translating ribosomes and the corresponding translational efficiency [23]. Several genome-wide translation analyses by ribosome profiling provide a list of genes that may have potential active uORFs mediating downstream CDS translational efficiency or encoding small peptides that may have biological

functions [17,24,25]. A previous ribosome profiling study in yeast by Ingolia et al. [17] hinted that uORFs of many genes may have a functional role in translational responses to acute amino acid starvation. Because amino acid deprivation is an important upstream signal that stimulates autophagy, we hypothesized that uORFs are involved in the translational control of autophagy.

To investigate the role of uORFs in core autophagy machinery in yeast, we initiated our analysis by extracting *ATG* genes from the subset of genes predicted to have active uORFs with the canonical start codon AUG based on ribosome profiling [17]. We found that *ATG5, ATG12, ATG13* and *ATG19* are highly likely to possess active uORFs (Table S1). However, no previous reports have associated uORFs with *ATG* genes. In addition, although uORFs are prominently more active in translation than other regions of the 5' UTR, their translational efficiencies are not comparable to the corresponding CDS. Indeed, some putative translational signals identified by ribosome profiling cannot be experimentally validated and might be false positives. Moreover, the functional activity of uORFs has been demonstrated for only a limited number of genes. Therefore, the reliability of the identification of uORFs and the mechanism of how the uORFs in specific genes regulate gene expression requires experimental evaluation.

Atg13 is an essential component of the Atg1 kinase complex that plays an irreplaceable role in autophagy initiation and in sensing upstream nutrient signals [26]. *ATG13* is predicted to possess a canonical uORF that initiates at an AUG codon in the 5' UTR and ends inside the downstream *ATG13* CDS (Figure 1A). This *ATG13* uORF encodes a 46-amino-acid polypeptide. To determine whether this canonical *ATG13* uORF plays a role in Atg13 translation, we constructed plasmids expressing either wild-type (WT) Atg13 tagged with the protein A (PA) epitope or a mutant version in which we mutated the AUG start codon of the *ATG13* uORF to UUG to prevent *ATG13* uORF translation. We then measured plasmid-based protein expression of Atg13-PA in *atg13Δ* cells. The *ATG13* uORF mutation resulted in a fold-change of approximately 2.3 in Atg13-PA protein level under nutrient-rich conditions (Figure 1B, 1C). Although nitrogen starvation stimulated Atg13-PA upregulation in WT cells, Atg13-PA levels were not significantly changed following 2 h of nitrogen starvation in cells with the *ATG13* uORF mutation. These results together demonstrate that the *ATG13* uORF is involved in controlling expression of *ATG13* in a nutrient-dependent manner.

Atg13 protein expression is controlled transcriptionally and post-transcriptionally. To exclude the potential effects of the *ATG13* uORF on *ATG13* transcription or mRNA stability, we measured the level of *ATG13* mRNA in WT cells and *ATG13* uORF mutant cells by real-time quantitative reverse transcription PCR (qRT-PCR). We found that the *ATG13* mRNA level was highly upregulated upon nitrogen starvation

as reported previously; however, there was no significant difference in the *ATG13* mRNA levels between WT cells and the cells with the *ATG13* uORF mutation (Figure 1D), demonstrating that the effect of the *ATG13* uORF on *ATG13* expression occurs most likely at the translational level.

The ATG13 *uORF is an inhibitory regulator for autophagy*

Because the *ATG13* uORF mutation led to an elevated level of Atg13-PA under nutrient-rich conditions relative to the WT, we speculated that the inhibitory uORF might therefore act as a regulator of autophagy. To investigate autophagy activity, we performed the quantitative Pho8Δ60 assay, in which we generated a mutant of the vacuolar phosphatase Pho8 that lacks the first 60 amino acids of its N terminus [27]. The mutant Pho8 can be delivered to the vacuole only through non-selective autophagy, which leads to the cleavage of its propeptide by vacuolar hydrolases and subsequent activation of its phosphatase activity. Hence, phosphatase activity in the Pho8Δ60 assay demonstrates autophagy flux in the cells. We observed a significant increase in autophagy activity in *ATG13* uORF mutant cells compared with WT cells after 3 h of nitrogen starvation (Figure 1E), suggesting that the elevated level of Atg13 allowed cells to initiate a more rapid autophagic response once shifted to nitrogen-starvation conditions.

To extend our analysis, we carried out the GFP-Atg8 processing assay. Atg8 is a ubiquitin-like protein required for autophagosome formation. Upon autophagy induction, the phosphatidylethanolamine (PE)-conjugated form of Atg8 initially resides on both sides of the phagophore; Atg8–PE on the outer surface of the mature autophagosome is recycled back into the cytosol, whereas the population inside the autophagosome is delivered to the vacuole and degraded. As GFP is relatively resistant to vacuolar hydrolases, the amount of free GFP generated by the GFP-Atg8 processing assay can be used to quantify autophagic delivery to the vacuole [28]. Consistent with the Pho8Δ60 assay results, we found that mutation of the *ATG13* uORF resulted in increased autophagy activity after 2 h of nitrogen starvation, as observed by the ratio of free GFP to GFP-Atg8 (Figure 1F, 1G).

Moreover, we tested Atg1 protein levels in WT and *ATG13* uORF mutant cells. Atg1 is a serine/threonine kinase that is essential for autophagosome formation. Atg13 physically interacts with Atg1, and the phosphorylation level of Atg13 affects Atg1 kinase activity and subsequent autophagy induction [29]. We found that Atg1 levels were not significantly changed by the *ATG13* uORF mutation in either nutrient-rich conditions or after 2 h of nitrogen starvation (Figure S1), excluding the possibility that the increased autophagy activity in *ATG13* uORF mutant cells is due to its impact on Atg1 protein levels. We also asked whether the observed increase in autophagy could be explained by enhanced Atg13 protein levels. We found that overexpression of Atg13-PA under the control of the *CUP1* promoter resulted in a higher level of autophagy as shown by Pho8Δ60 activity (Figure S2), indicating that elevated Atg13 levels contribute to autophagy activation. Collectively, our results indicate that the translational

upregulation of *ATG13* mediated by bypassing the uORF promotes autophagy.

Translational control of ATG13 *by its uORF is dependent on a partial Kozak sequence and Gcn2 kinase*

Next, we asked how the identified *ATG13* uORF regulates Atg13 translation. It is commonly acknowledged that when uORFs show a repressive effect in CDS translation, it is presumably because the translation of uORFs can occur at the expense of reducing translation initiation of the downstream CDS [30]. During translation, the GTP-bound eIF2 complex binds the initiator methionyl-tRNA (Met-tRNA$_i^{Met}$) to form the ternary complex eIF2-GTP-Met-tRNA$_i^{Met}$, and subsequently interacts with the 40S ribosomal subunit, Tif11/eIF1A and the eIF3 complex to assemble into the 43S pre-initiation complex (PIC) [31]. Starting from the 5' ends of mRNAs, the PIC scans for a start codon, which is usually the first AUG base pairing with Met-tRNA$_i^{Met}$, in the 5' to 3' direction. Once the start codon is identified, GTP is hydrolyzed by eIF2, causing the eIF proteins to dissociate from the PIC, which allows the joining of the 60S ribosomal subunit to form an 80S ribosome; translation elongation then begins with the decoding of the second codon [31].

In addition to the activity of the PIC, the context of nucleotides of the start codons, such as the Kozak sequence, plays an important role to strengthen or weaken start codon recognition. An optimal Kozak consensus sequence is defined as GCCA/GCC**AUG**G, where the A of the AUG start codon (bold) is designated +1, a purine is present at position −3 (underlined) and a guanosine is present at +4 (underlined) [32]. This optimal Kozak sequence provides stabilizing interactions with the PIC, and hence dictates a strong recognition context for the start codon. The correct AUG for the *ATG13* CDS follows these rules for an optimal Kozak sequence (Figure 2A). In contrast, the *ATG13* uORF possesses a relatively weak Kozak sequence with an A at position +4. Hence, we hypothesized a leaky scanning model for uORF-mediated Atg13 translation. In the leaky scanning model, AUG start codons within uORFs that are present within a weak Kozak sequence may be recognized, starting the translation of the uORF, or "scanned through" meaning this start codon is bypassed. In the latter situation, translation efficiency of the downstream CDS is elevated.

To test whether the initiation context of the uORF start codon affects Atg13 translation, we constructed strains with either 1) a mutated initiation sequence for the *ATG13* uORF, converting A to U in the AUG codon, or 2) a mutation in the Kozak sequence converting A to U at position −3 (Figure 2A). We found that the mutation in the Kozak sequence led to increased Atg13-PA translation similar to the level of a direct mutation in the *ATG13* uORF start codon (Figure 2B). Moreover, we measured GFP-Atg8 processing to determine the effect of the mutations on autophagy activity. We found that Kozak mutant cells displayed increased levels of autophagy to a similar extent as uORF mutant cells (Figure 2B). As a control, we mutated an AGG codon to UUG in the 5' UTR of the *ATG13* mRNA transcript that is 46 nucleotides
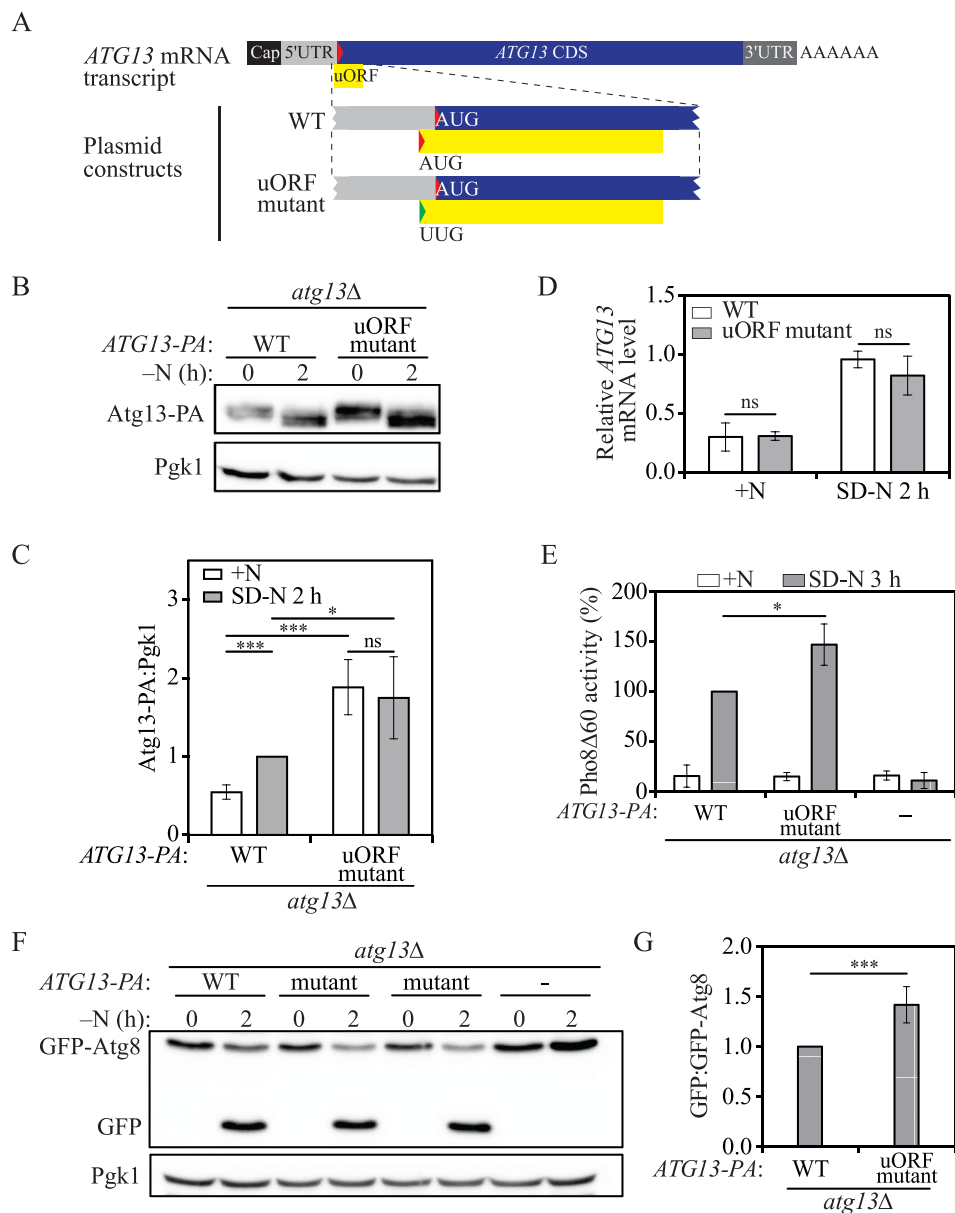
Figure 1. An *ATG13* uORF regulates autophagy under nitrogen-starvation conditions in yeast. (A) Schematic representation of *ATG13* mRNA transcript with a potential functional uORF identified by ribosome profiling (yellow box). This *ATG13* uORF has a start codon (AUG) in the 5' UTR, and in-frame stop codon preceding the end of the *ATG13* CDS. The mutation made in the start codon of the *ATG13* uORF in the plasmid construct is shown as indicated (represented by the change from a red triangle to a green triangle). (B) Atg13-PA levels were measured by western blot in WT and *ATG13* uORF mutant cells under growing conditions and after 2 h of nitrogen-starvation conditions. Pgk1 was used as a loading control. (C) The ratio of Atg13-PA to Pgk1 was quantified. Mean±SD of $n = 3$ independent experiments are shown as indicated. Student's t-test; ns: not significant, **: $p < 0.01$, ***: $p < 0.005$. (D) *ATG13-PA* mRNA levels were determined in WT and *ATG13* uORF mutant cells under growing and 1-h nitrogen-starvation conditions by RT-qPCR. Mean±SD of $n = 3$ independent experiments are shown as indicated. ANOVA; ns: not significant. (E) Autophagy activity was measured with the Pho8Δ60 assay in WT, *ATG13* uORF mutant, and *atg13Δ* strains under growing conditions and after 3 h of nitrogen starvation. Mean±SD of $n = 3$ independent experiments are shown as indicated. Student's t-test; *: $p < 0.05$. (F) Autophagy was measured using the GFP-Atg8 processing assay in WT, *ATG13* uORF mutant and *atg13Δ* strains under growing conditions and after 2 h of nitrogen starvation; a representative image is shown. (G) The ratio of free GFP to GFP-Atg8 after 2 h of nitrogen starvation was quantified. Mean±SD of $n = 3$ independent experiments are shown as indicated. Student's t-test; ***: $p < 0.005$. SD-N, synthetic minimal medium lacking nitrogen; +N (YPD), yeast extract-peptone-dextrose; WT, wild type; PA, protein A.

upstream of the uORF start codon. The control mutant showed similar Atg13-PA protein levels as WT cells (Figure 2C). These results suggest that the partial Kozak sequence for the start codon of the *ATG13* uORF is essential for regulating uORF-mediated Atg13 translation.

Although the partial Kozak sequence for the *ATG13* uORF affects Atg13 translation, suggesting a leaky scanning mechanism, we also examined the role of Gcn2, which is typically involved in translation reinitiation. Previous studies showed that upon amino acid starvation, the protein kinase Gcn2 phosphorylates Sui2/eIF2α, and hence inhibits the formation of new ternary complexes, thus impeding the reinitiation of translation at the CDS after ribosome termination [6,33]. To further explore the mechanism of the *ATG13* uORF, we deleted *GCN2* in WT and *ATG13* uORF mutant cells expressing Atg13-PA.

In the cells expressing WT Atg13-PA, 2-h nitrogen starvation led to the expected increase in Atg13-PA levels; however, Gcn2 deficiency led to diminished Atg13-PA protein levels under 2-h nitrogen starvation conditions (Figure 2D, 2E, Figure S3), indicating that Gcn2 mediates translational expression of Atg13 under these conditions. In contrast, Atg13-PA protein levels were not significantly affected by *GCN2* knockout in *ATG13* uORF mutant cells under identical nitrogen-starvation conditions, suggesting that the bypass of uORF-mediated Atg13 translational regulation in WT cells upon nitrogen starvation was Gcn2 dependent. These results together indicate that the *ATG13* uORF regulates Atg13 expression through a Gcn2-dependent mechanism.

Multiple inhibitory *ATG5* uORFs mediates Atg5 translation and autophagy regulation

Atg5 is an essential protein involved in the process of phagophore expansion and autophagosome formation [34,35]. During autophagy, Atg5 is covalently conjugated with Atg12 [35]. The resulting irreversible Atg12–Atg5 conjugate functions as an E3-like enzyme to facilitate Atg8 lipidation [36]. *ATG5* is predicted to have five potential canonical uORFs (Table S1). We investigated four of these putative uORFs, which have been shown to actively bind to translating ribosomes. All these uORFs have both start and stop codons located inside the 5′ UTR of *ATG5* (Figure 3A). The most

upstream of these sites, uORF1, encodes a 13 amino-acid polypeptide and its corresponding stop codon is 33 nucleotides ahead of the downstream *ATG5* CDS. uORF2 encodes a 16 amino-acid polypeptide and its corresponding stop codon is 8 nucleotides ahead of the downstream *ATG5* CDS. uORF3 and uORF4 share the same stop codon and encode extremely small peptides with a length of 2 or 1 amino acids, respectively.

To study the roles of each individual uORF in Atg5 translation, we constructed plasmids that express either WT Atg5-PA or a mutant version by switching the start codons of uORF1, uORF2 or both uORF3 and uORF4 from AUG to UUG (Figure 3B); uORF3 and uORF4 were mutated together because they partially overlap and share the same stop codon. These plasmids were then transformed into *atg5Δ* cells. We named the cells with mutated uORF1 and mutated uORF2 "mut 1" and "mut 2", respectively, whereas those expressing mutated uORF3 and uORF4 were named "mut 3".

To exclude the possibility that these *ATG5* uORFs have a role in *ATG5* transcription or mRNA stability, we first performed RT-qPCR. No significant difference in *ATG5* mRNA levels was detected among the WT and mutant strains under both growing and nitrogen-starvation conditions (Figure 3C). Next, we measured Atg5-PA levels by western blot. Atg5-PA has two forms on the blot: the free form of Atg5-PA and the Atg12–Atg5-PA conjugate. We first focused on total Atg5-PA (free Atg5-PA+Atg12–Atg5-PA) levels to
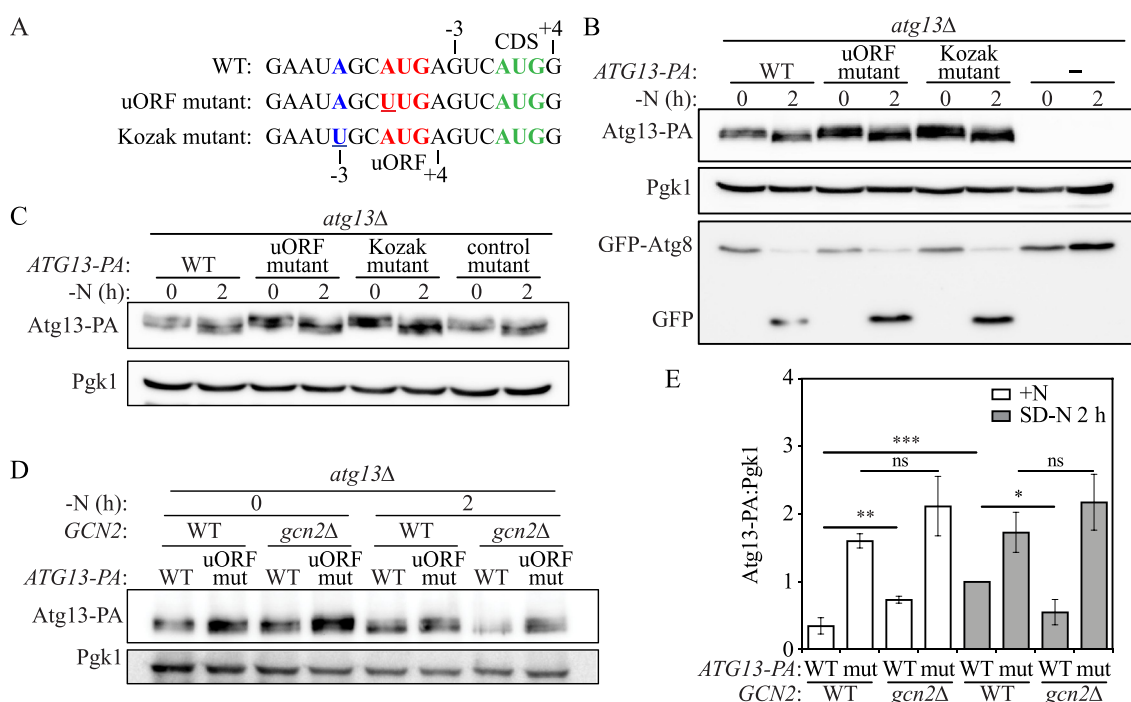
Figure 2. uORF-mediated Atg13 translation is Gcn2 dependent. (A) The mutations made in the Kozak mutant and uORF mutant cells are shown as indicated; mutated regions are presented in blue and red colors and mutated nucleotides are underlined. The correct AUG start codon of the *ATG13* CDS is presented in green. (B) Atg13-PA protein levels and autophagy activity were measured by western blot and GFP-Atg8 processing in *atg13Δ* strains with empty vector or vectors expressing WT Atg13-PA, an *ATG13* uORF mutant, or a Kozak mutant under growing and 2-h nitrogen-starvation conditions. (C) Atg13-PA protein levels were measured in *atg13Δ* strains with vectors expressing WT Atg13-PA, an *ATG13* uORF mutant, a Kozak mutant, or a control mutant under growing and 2-h nitrogen-starvation conditions. (D) Atg13-PA protein levels were measured by western blot in either *atg13Δ* or *atg13Δ gcn2Δ* cells expressing WT Atg13-PA or an *ATG13* uORF mutant under growing and 2-h nitrogen-starvation conditions; a representative image is shown. (E) The ratio of Atg13-PA to Pgk1 was quantified. Mean±SD of *n* = 3 independent experiments are shown as indicated. Student's *t*-test; *: $p < 0.05$, **: $p < 0.01$, ***: $p < 0.005$, ns: not significant. SD-N, synthetic minimal medium lacking nitrogen; +N (YPD), yeast extract-peptone-dextrose; WT, wild type; PA, protein A.

explore the role of the *ATG5* uORFs on Atg5 translation. All three mutant cells showed increased total Atg5-PA levels under growing conditions compared with WT cells (Figure 3D, 3E). Although total Atg5-PA levels of WT cells were significantly increased after 2 h of nitrogen starvation, we did not find significant changes of the total Atg5-PA levels between growing and starvation conditions in any of the mutant cells. These results suggest that these four predicted uORFs are involved in downregulating *ATG5* under growing conditions.

Moreover, no significant difference was observed following 2 h of starvation in strains with either uORF1 or uORF2 mutation relative to the WT (Figure 3D, 3E), suggesting that the disruption of either *ATG5* uORF1 or uORF2 eliminated the entire inhibitory role of *ATG5* uORFs in the regulatory mechanism of translation. In contrast, double mutations in uORF3 and uORF4 resulted in higher levels of Atg5-PA compared with the other two mutants. This difference may reflect the relative position of uORF3 and uORF4; the corresponding stop codon ends just 3 nucleotides before the start codon of the *ATG5* CDS, and the short distance would provide less time for the 40S ribosome to reassemble factors needed for reinitiation after translation termination at either of these uORFs.

The formation of the Atg12–Atg5 conjugate is essential for autophagy [37]. We found that Atg12–Atg5-PA levels in mut 1, mut 2 and mut 3 resulted in fold-changes of 2.6-, 3.2-, and 2.7 relative to WT cells in nutrient-rich conditions (Figure 3D, 3F). The Atg12–Atg5 levels in WT cells quickly increased to that of the three mutant strains after 2 h of starvation, at which time the conjugation appeared to be saturated. Next, we examined the effect of the uORF mutants on autophagy activity using the Pho8Δ60 assay. None of the three mutants showed a significant difference in autophagy activity compared with the WT after 3 h of starvation (Figure S4), presumably because the Atg12–Atg5-PA levels in WT cells reached the saturation point within 2 h of starvation (Figure 3D, 3F). To further examine our hypothesis, we took advantage of the shorter time course that is possible with the GFP-Atg8 processing assay. In contrast to the results seen with the Pho8Δ60 assay, we found an ~40% increase in autophagy activity in both the uORF1 and uORF2 mutant strains following 1.5 h of starvation (Figure 3H, 3I); there was no detectable increase in the strains containing double mutations in uORF3 and uORF4. To reconcile these differences, we extended our analysis by performing a short-term Pho8Δ60 assay with a time course closer to that of the GFP-Atg8 processing assay. We found that consistent with the latter, after 1.5 h of starvation, the uORF1 and uORF2 mutant strains showed elevated autophagy activity (Figure 3G). These data collectively suggest that *ATG5* uORF1 and uORF2 play a predominant role in autophagy regulation compared with uORF3 and uORF4, even though the latter have a more pronounced effect on the level of free Atg5.

Atg12 and Atg19 are translationally regulated by uORFs

Based on the above findings for Atg5 and Atg13, we decided to examine the potential roles of the predicted canonical uORFs of *ATG12* and *ATG19*, to determine whether they may also play an inhibitory role in translation regulation. As mentioned above, Atg12 is a component of the Atg12–Atg5 conjugate, the formation of which is essential for autophagosome formation [36]. Atg19 is a receptor protein for the cytoplasm-to-vacuole targeting (Cvt) pathway, a type of selective autophagy that specifically delivers certain resident hydrolases into the yeast vacuole [38]. The predicted *ATG12* uORF encodes a 3-amino-acid peptide, and its stop codon is inside the downstream CDS (Figure 4A). The *ATG19* 5' UTR contains three putative uORFs (Table S1). We studied the only *ATG19* uORF that contains a suboptimal Kozak sequence surrounding its start codon. A previous study that exploits computer simulations to model scanning and ribosomal translational elongation behavior showed that the uORFs with a greater length are more likely to display inhibitory effects of downstream CDS translation [39]. The potential *ATG19* uORF is relatively longer with a length of 15 amino acids and ends 48 nucleotides before the *ATG19* CDS. We constructed plasmids expressing WT Atg12-PA or WT Atg19-PA, or their uORF mutant versions by changing the corresponding uORF start codons from AUG to UUG. These plasmids were transformed into *atg12Δ* or *atg19Δ* cells, respectively.

To examine the role of the *ATG12* and *ATG19* uORFs on translation, we measured protein levels by western blot. *ATG12* uORF mutant cells displayed a fold-change of 2.3 and 1.7 in Atg12-PA levels compared with WT cells in nutrient-rich conditions and after 2 h of nitrogen starvation, respectively (Figure 4B, 4C), implying that the *ATG12* uORF controls Atg12-PA levels under both conditions. *ATG19* uORF mutant cells demonstrated a fold-change of 1.9 and 1.3 in Atg19-PA levels compared with WT cells in nutrient-rich and nitrogen starvation conditions, respectively (Figure 4D, 4E), indicating a similar regulatory role as seen with the *ATG12* uORF. To determine if the *ATG12* and *ATG19* uORFs affect corresponding mRNA stability, we measured mRNA levels by RT-qPCR. Under either nutrient-replete or nitrogen-starvation conditions, the mutations of the uORF start codons did not significantly change *ATG12* or *ATG19* mRNA levels (Figure 4F, 4G). These data suggest that the *ATG12* and *ATG19* uORFs repress their corresponding CDS translation.

More than 20 ATG genes have potential active uORFs (canonical and non-canonical) in human

Next, we asked whether uORFs play a role in the translational control of *ATG* genes in more-complex eukaryotes. Recently, several genome-wide ribosome profiling studies were performed in human cells [25,40,41]. Active uORFs widely exist in the human genome; however, the precise number and roles of the uORFs are unknown. A previous study by McGillivray et al. exploited machine learning algorithm training based on uORFs labeled within ribosome profiling experiments to predict potential active uORFs that are bound by ribosomes in human cells [25].

To gain a comprehensive scope of uORF-mediated translation regulation of *ATG* genes in human, we extracted the
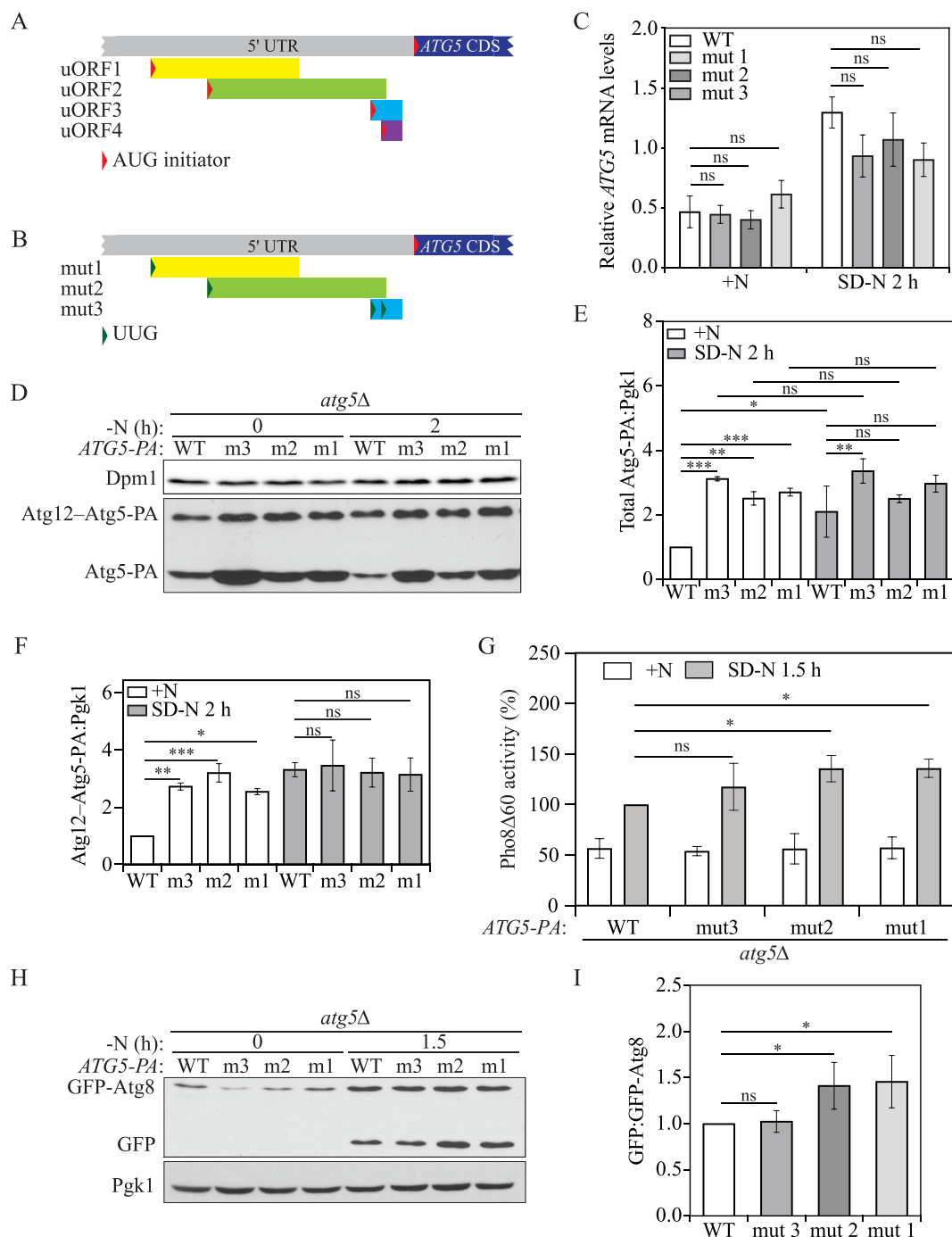
Figure 3. Multiple *ATG5* uORFs mediate Atg5 translation and autophagy in yeast. (A) Schematic representation of partial *ATG5* mRNA transcript with 4 potential functional uORFs identified by ribosome profiling (represented by yellow, blue, green, and purple boxes). Each *ATG5* uORF has a start codon (AUG) in the 5′ UTR, and a stop codon preceding the *ATG5* CDS. (B) The mutations made in the start codon of *ATG5* uORFs in the plasmid constructs are shown as indicated (represented as a change from a red triangle to a green triangle). (C) *ATG5-PA* mRNA levels were determined in WT and *ATG5* uORF mutant cells under growing and 1-h nitrogen-starvation conditions by RT-qPCR. Mean±SD of $n = 3$ independent experiments are shown as indicated. ANOVA; ns: not significant. (D) Atg5-PA levels were measured by western blot in WT and *ATG5* uORF mutant cells under growing conditions and after 2 h of nitrogen starvation. Pgk1 was used as a loading control. (E) The ratio of total Atg5-PA to Pgk1 was quantified. Mean±SD of $n = 3$ independent experiments are shown as indicated. ANOVA; ns: not significant, *: $p < 0.05$, **: $p < 0.01$, ***: $p < 0.005$. (F) The ratio of Atg12–Atg5-PA to Pgk1 was quantified. Mean±SD of $n = 3$ independent experiments are shown as indicated. ANOVA; ns: not significant, *: $p < 0.05$, **: $p < 0.01$, ***: $p < 0.005$. (G) Autophagy activity was measured using the Pho8Δ60 assay in WT, and *ATG5* uORF mutant cells under growing conditions and after 3 h of nitrogen starvation. Mean±SD of $n = 3$ independent experiments are shown as indicated. ANOVA; *: $p < 0.05$, ns: not significant. (H) Autophagy was measured with the GFP-Atg8 processing assay in WT, and *ATG5* uORF mutant strains under growing conditions and after 1.5 h of nitrogen starvation; a representative image is shown. (I) The ratio of free GFP to GFP-Atg8 after 1.5 h of nitrogen starvation was quantified. Mean±SD of $n = 3$ independent experiments are shown as indicated. ANOVA; *: $p < 0.05$. SD-N, synthetic minimal medium lacking nitrogen; +N (YPD), yeast extract-peptone-dextrose; WT, wild type; PA, protein A.

genes encoding core autophagy machinery from the list of genes with potential active uORFs predicted in the study by McGillivray et al. [25]. The set of core *ATG* genes used here encodes 5 groups of proteins, including 1) the ULK1 kinase complex, composed of ULK1, ULK2, RB1CC1/FIP200, ATG13, and ATG101; 2) the class III phosphatidylinositol 3-kinase (PtdIns3K) complex, which is composed of BECN1/Beclin 1, PIK3C3/VPS34, PIK3R4/VPS15, ATG14,

NRBF2, and UVRAG; 3) the ATG9 trafficking system, which is composed of ATG2A, ATG2B, WIPI1, WIPI2, WDR45/WIPI4 and the transmembrane protein ATG9A; 4) the Atg8-family ubiquitin-like (Ubl) conjugation system, composed of ATG4A, ATG4B, ATG4C, ATG4D, ATG3, MAP1LC3A, MAP1LC3B, MAP1LC3C, GABARAP, and GABARAPL2; 5) the ATG12 Ubl conjugation system, composed of ATG5, ATG12, ATG16L1, ATG7, and ATG10 [3,42]. We provide the list of uORFs predicted to be active for ATG genes in Table S2. We found that among the 32 chosen genes, 18 of them possess one or more canonical uORFs with an AUG start codon (Figure 5A). We noticed that ATG5 had 3 potential AUG-initiated uORFs, whereas ATG12, and ATG13 did not display the existence of uORFs with AUG start codons.

Several prior studies revealed that in addition to canonical AUG start codons, numerous uORFs initiate with non-AUG start codons, including ACG, AUU, AUA, AUC, CUG, GUG and UUG [43,44]. We therefore decided to examine whether ATG12, ATG13 and other human ATG genes exploit non-canonical uORFs, which initiate with a non-AUG start codon, to regulate their translation. Hence, we determined the composition of potential active uORFs (including uORFs that started with AUG and near-cognate start codons) of ATG genes. We found that 27 out of 32 human ATG genes have at least one predicted functional uORF (Figure 5B). ATG5, ATG12, and ATG13 have 46, 4 and 29 uORFs, respectively. AUG has been identified as the most prevalent uORF start codon in the genome [25]. However, our analysis of the data from McGillivray et al. [25] indicated that uORFs for ATG genes exhibit translation initiation mostly at CUG and GUG
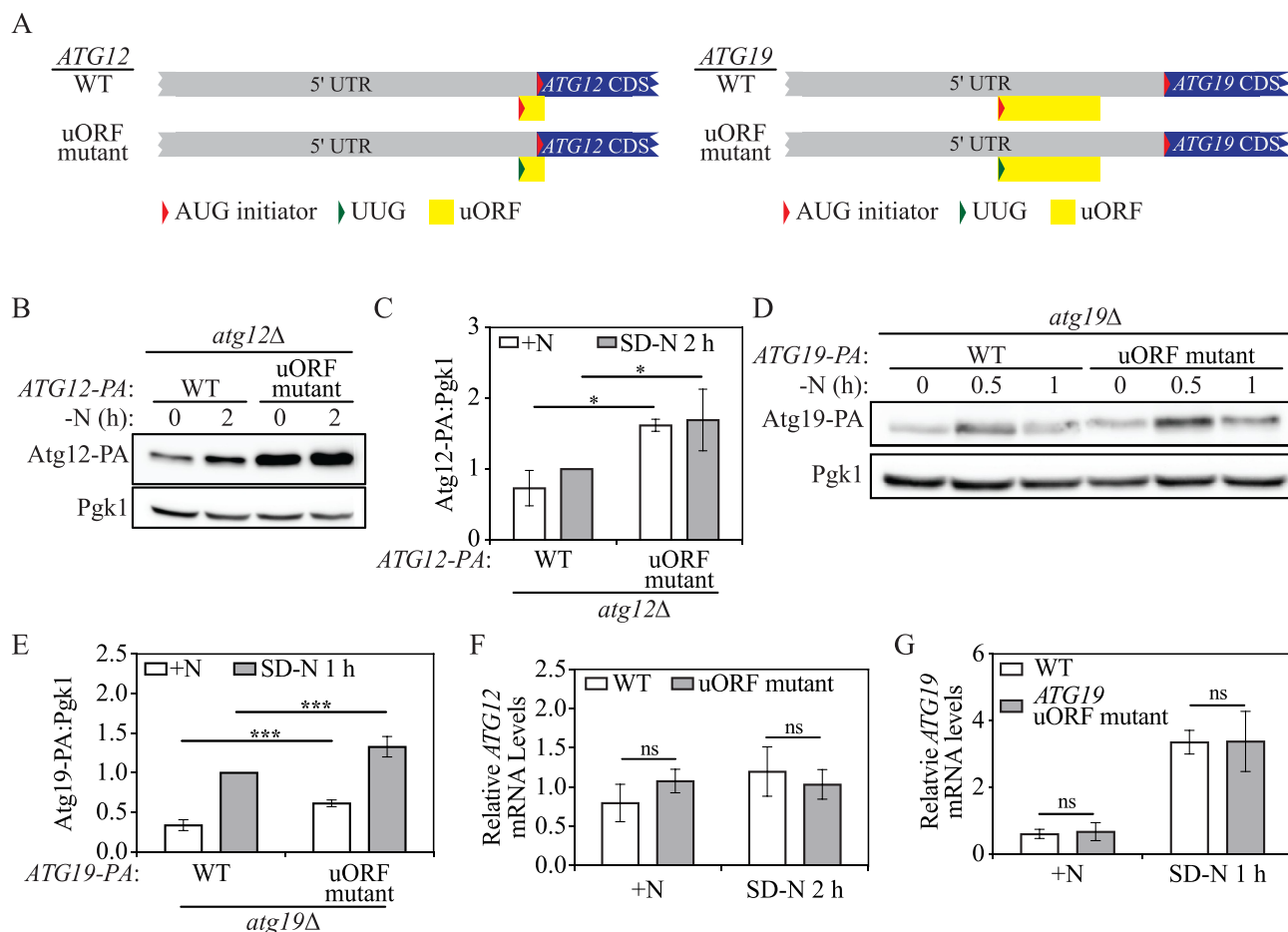
Figure 4. Yeast Atg12 and Atg19 translation are mediated by a single inhibitory uORF in the corresponding 5′ UTR. (A) Schematic representation of partial ATG12 or ATG19 mRNA transcripts with a potential functional uORF identified by ribosome profiling (yellow box). The ATG12 uORF has a start codon (AUG) in the 5′ UTR, and an in-frame stop codon preceding the end of the ATG12 CDS. The ATG19 uORF has a start codon (AUG) in the 5′ UTR, and a stop codon preceding the ATG19 CDS. The mutations made in the start codon of the ATG12 or ATG19 uORF in the plasmid constructs are shown as indicated (represented as a change from a red triangle to a green triangle). (B) Atg12-PA levels were measured by western blot in WT and ATG12 uORF mutant cells under growing conditions and after 2 h of nitrogen starvation. Pgk1 was used as a loading control. (C) The ratio of Atg12-PA to Pgk1 was quantified. Mean±SD of $n = 3$ independent experiments are shown as indicated. ANOVA; *: $p < 0.05$. (D) Atg19-PA levels were measured by western blot in WT and ATG19 uORF mutant cells under growing conditions and after 0.5 h and 1 h of nitrogen starvation. (E) The ratio of total Atg19-PA to Pgk1 under growing and 1-h nitrogen-starvation conditions was quantified. Mean±SD of $n = 4$ independent experiments are shown as indicated. ANOVA; ***: $p < 0.005$. (F) ATG12-PA mRNA levels were determined in WT and ATG12 uORF mutant cells under growing and 2-h nitrogen-starvation conditions by RT-qPCR. Mean±SD of $n = 3$ independent experiments are shown as indicated. ANOVA; ns: not significant. (G) ATG19-PA mRNA levels were determined in WT and ATG19 uORF mutant cells under growing and 1-h nitrogen-starvation conditions by RT-qPCR. Mean±SD of $n = 3$ independent experiments are shown as indicated. ANOVA; ns: not significant. SD-N, synthetic minimal medium lacking nitrogen; +N (YPD), yeast extract-peptone-dextrose; WT, wild type; PA, protein A.

(Figure 5C). CUG and GUG are more likely to be scanned through/bypassed during start codon recognition, suggesting that leaky scanning is a common feature in the repressive mechanism for uORF-mediated translational control of *ATG* genes.

Identification of singleton variants provides tremendous information for human phenotypic variation and disease susceptibility [45]. We scanned singleton variants on start codons of predicted uORFs of *ATG* genes from the ExAc catalog [25,46]. We found that 10 genes encoding core autophagy machinery, including *ULK2, RB1CC1/FIP200, PIK3C3/VPS34, ATG14, NRBF2, ATG5, ATG10, ATG4C, MAP1LC3A* and *MAP1LC3B*, are associated with altered start codons of predicted active uORFs at a low allele mutation frequency (from $8.24e^{-06}$ to $1.04e^{-05}$) (Table S3, Figure 5D). These data imply that there is a high possibility that the predicted uORFs in these *ATG* genes are active and functionally important, because a lower frequency of singletons is often due to heavy selection pressure of regions with essential functions [47].

Non-canonical uORFs regulate starvation-induced ATG4B and ATG12 translation in human

Among the four members of the ATG4 family (ATG4A, ATG4B, ATG4C, and ATG4D), the role of ATG4B is best characterized. ATG4B is a crucial cysteine protease that proteolytically cleaves Atg8-family proteins (LC3 and GABARAP subfamilies) to their active forms and promotes efficient autophagosome biogenesis [48]. We noticed that *ATG4B* is predicted to have only one active non-canonical uORF that initiates with a UUG codon and partially overlaps with the downstream CDS (Figure 6A). To validate the function of this single uORF in ATG4B expression regulation, we generated constructs with a luciferase reporter coding sequence downstream of the *ATG4B* 5' UTR containing either the WT predicted active *ATG4B* uORF or a mutant version with the start codon changed from UUG to AAG. We chose AAG because a previous study suggested that AAG is employed as the start codon of uORFs with the least probability of function [49]. The constructs containing WT *ATG4B* 5'UTR-LUC and uORF mutant *ATG4B* 5'UTR-LUC were transfected into 293 FT cells.

To investigate whether and how the *ATG4B* uORF affects protein translation upon stress, we determined the luciferase activity and luciferase mRNA levels under nutrient-rich conditions or after 4 h of Hanks' balanced salt solution (HBSS)-mediated starvation. The luciferase mRNA level was not affected by mutation of the *ATG4B* uORF during either growing or starvation conditions (Figure 6B), suggesting the *ATG4B* uORF does not affect mRNA stability. However, the cells with the mutant construct displayed a fold-increase of 2.4 and 2.0 in luciferase activity compared with WT cells under nutrient-rich and HBSS starvation conditions, respectively (Figure 6C). These results indicate that the *ATG4B* uORF inhibits downstream ORF translation under both conditions.

Although human ATG12 is highly conserved down to yeast Atg12 in terms of structure and function [50,51], human

ATG12 mRNA was not predicted to possess a canonical uORF as seen with yeast *ATG12*. Instead, *ATG12* had four predicted non-canonical uORFs, all of which initiate with non-AUG codons, in the order of CUG, GUG, ACG, and UUG from 5' to 3' (Figure 6A). We named the four non-canonical uORFs as uORF1, uORF2, uORF3 and uORF4 based on the order of start codon positions from 5' to 3'. To determine the role of each *ATG12* uORF in translational regulation, we constructed a WT *ATG12* 5' UTR-LUC plasmid that contains the luciferase reporter coding sequence downstream of the *ATG12* 5' UTR. We then generated a set of mutant plasmids by mutating the start codon of each predicted uORF to AAG. These constructs were again transfected into 293 FT cells.

We first measured luciferase mRNA levels by RT-qPCR. Luciferase mRNA levels were not affected by mutation in any of the *ATG12* uORFs during either growing or 4-h HBSS starvation conditions (Figure 6D), demonstrating no effect of *ATG12* uORFs on mRNA stability. Next, we examined luciferase activity as a readout of translation activity. During growing conditions, mutations in uORF1 or uORF2 did not significantly change luciferase activity, whereas mutations in uORF3 and uORF4 resulted in a fold-increase of 3.27 and 2.81, respectively (Figure 6E). Upon 4 h of HBSS starvation, we observed a fold-increase of 1.82, 2.11, 3.57 and 3.35 in luciferase activity in the cells with mutations in the start codons of uORF1 to uORF4, respectively. Collectively, these results indicate that the *ATG12* uORF3 and uORF4 are predominant *cis* regulators for downstream ORF translation, although *ATG12* uORF1 and uORF2 displayed a mild inhibitory effect on translation.

Discussion

Though substantial effort has been made to delineate the mechanisms for how *ATG* genes are regulated transcriptionally and post-translationally, little is known about how *ATG* genes bypass the general translation suppression that occurs during stress conditions to maintain the activation of autophagy. In this study, we proposed and validated the hypothesis that uORFs act as an important regulatory element for the translation of *ATG* genes, especially in response to starvation, controlling proteins that participate in different stages of autophagy, including initiation, phagophore expansion, and cargo selection.

We first hypothesized that the canonical *ATG13* uORF mediates Atg13 translation through a leaky-scanning mechanism and showed that the suboptimal Kozak sequence for the *ATG13* uORF is involved in regulation of Atg13 translation. However, the +4 position in the Kozak sequence may not play as much of a role as the −3 position [52]. Thus, depending on the relative importance of the −3 and +4 positions, if we consider the *ATG13* uORF to have an optimal Kozak sequence, the likelihood of a leaky-scanning mechanism is decreased. Accordingly, we also considered whether the *ATG13* uORF exploits a translation reinitiation mechanism. The reinitiation model was proposed by Kozak and suggests that when there is a relatively long distance between a uORF and the downstream ORF, the ribosomes are able to
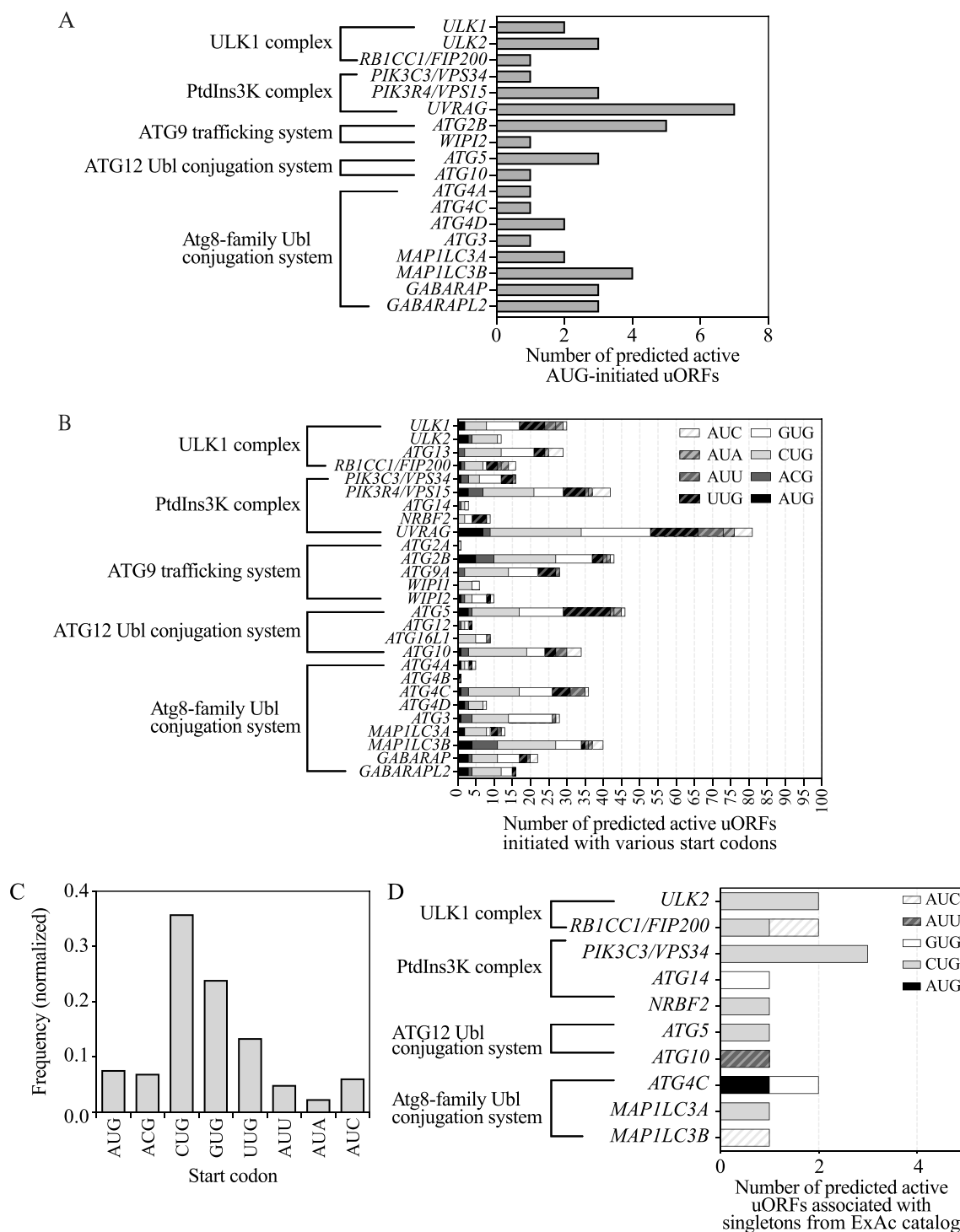
Figure 5. More than 20 human *ATG* genes are predicted to have functional uORFs. (A) The number of active canonical uORFs initiated with an AUG start codon for *ATG* genes predicted by a machine learning algorithm [25]. *ATG* genes are classified into 5 groups, including those encoding components of the ULK1 complex, the PtdIns3K complex, the ATG9 trafficking system, the ATG12 Ubl conjugation system, and the Atg8-family Ubl conjugation system. *ATG* genes with no active canonical uORFs are not shown. (B) Composition analysis of uORFs (initiated with AUG or near-cognate start codons) in *ATG* genes predicted by a machine learning algorithm [25]. *ATG* genes with no active uORFs are not shown. (C) The frequency of AUG start codons and near-cognate start codons of predicted positive uORFs in all *ATG* genes. (D) Ultra-rare variants (singletons) from the Exome Aggregation Consortium (ExAC) catalog v.1 that are associated with predicted active uORFs of *ATG* genes are counted [25,46]. The composition of uORFs (initiated with AUG and near-cognate codons) that are associated with singleton variants are analyzed. PtdIns3K, phosphatidylinositol 3-kinase; Ubl, ubiquitin-like.

reassemble along with initiation factors and initiate the translation of the downstream ORF [32]. Our data fit either mechanism, but we think there is a low probability that this *ATG13* uORF exploits a reinitiation mechanism; reinitiation is found to be highly inefficient when the two ORFs are located very close together, within 8 nucleotides, or overlap with each

other [53]. In addition, the reinitiation model is based on the presence of a termination site downstream of the uORF, but upstream of the canonical ORF. Considering that the identified *ATG13* uORF in this study ends inside the *ATG13* CDS, we think that the reinitiation model is not likely to be used. The main piece of data that would seem to argue against the
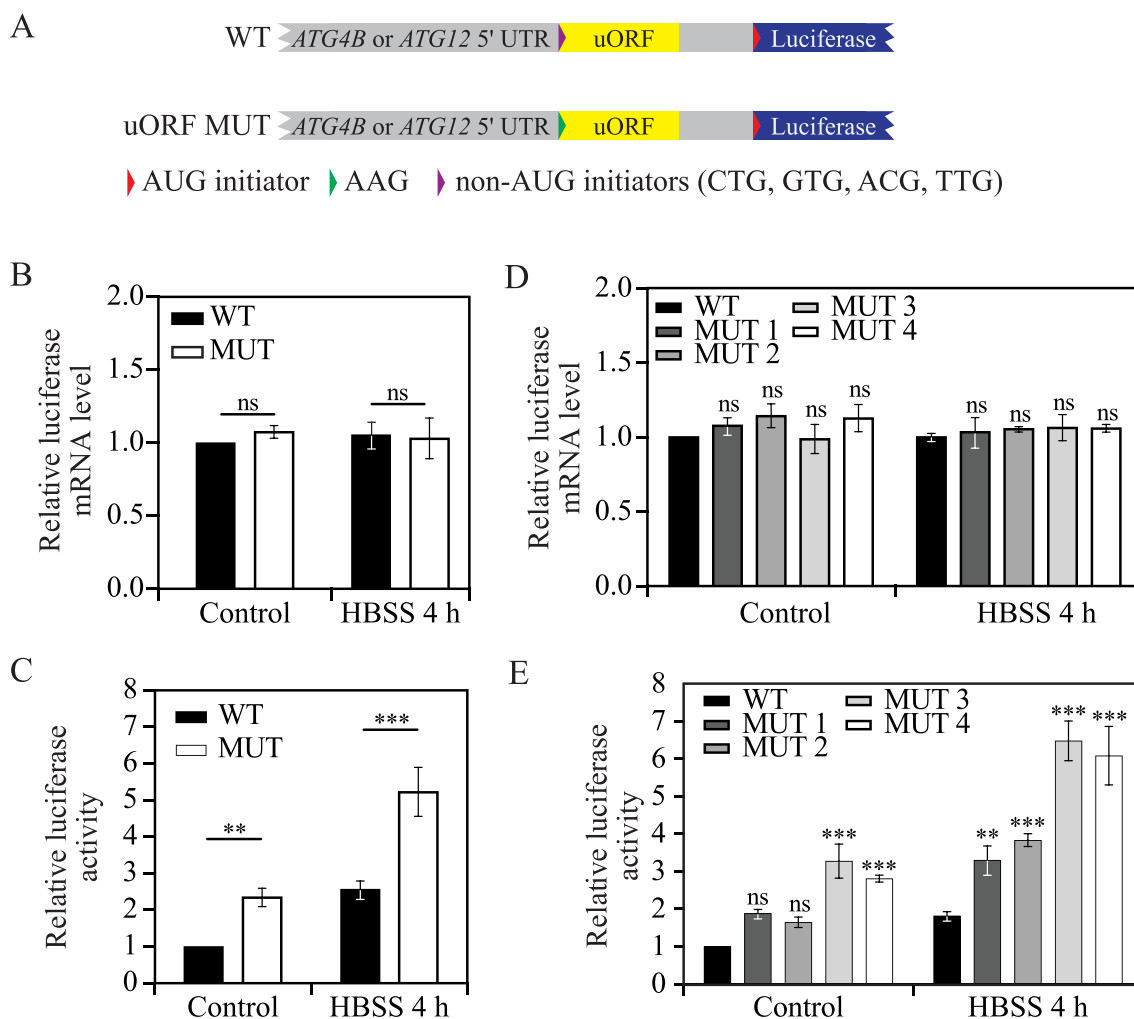
Figure 6. Non-canonical uORFs regulate ATG4B and ATG12 translation in human. (A) Schematic representation of WT and mutant human *ATG12* or *ATG4B* 5'UTR-LUC constructs. *ATG12* or *ATG4B* 5′ UTR-containing uORFs (yellow box) with non-AUG start codons (purple triangle) were cloned upstream of the luciferase CDS in WT constructs. The start codons of the uORFs were changed to AAG (green triangle) in the mutant constructs. (B) Relative luciferase mRNA levels were measured in 293 FT cells transfected with WT and uORF mutant *ATG4B* 5'UTR-LUC constructs under control (nutrient-rich medium) and 4-h HBSS starvation conditions. Mean±SD of $n = 3$ independent experiments are shown as indicated. ANOVA; ns: not significant. (C) Relative luciferase activities were measured in 293 FT cells transfected with WT and uORF mutant *ATG4B* 5'UTR-LUC constructs under control (nutrient-rich medium) and 4-h HBSS starvation conditions. Mean±SD of $n = 3$ independent experiments are shown as indicated. ANOVA; **: $p < 0.01$, ***: $p < 0.005$. (D) Relative luciferase mRNA levels were measured in 293 FT cells transfected with WT and uORF mutant (MUT 1 to MUT 4) *ATG12* 5'UTR-LUC constructs as in (B). Mean±SD of $n = 3$ independent experiments are shown as indicated. ANOVA; ns: not significant. (E) Relative luciferase activities were measured in 293 FT cells transfected with WT and uORF mutant (MUT 1 to MUT 4) *ATG4B* 5'UTR-LUC constructs as in (C). Mean±SD of $n = 3$ independent experiments are shown as indicated. ANOVA; **: $p < 0.01$, ***: $p < 0.005$. WT, wild type; HBSS, Hanks' balanced salt solution.

leaky-scanning model is the finding that Gcn2 is required to bypass the uORF-mediated decrease in translation. However, the general regulation of *ATG* gene expression is typically opposite that of most other genes. That is, under starvation conditions approximately 98% of the genes in a cell are downregulated, whereas *ATG* genes are upregulated. Along these lines, factors that promote the expression and translation of genes in growing conditions, such as TOR, often act in the opposite manner for *ATG* genes. Although we do not know the precise mechanism, we hypothesize that Gcn2 may be acting in this way, participating in the downregulation of most genes under starvation conditions, while facilitating the expression of *ATG* genes. Thus, we hypothesize that the decreased availability of ternary complexes mediated by Gcn2 upon starvation contributes to the leaky scanning mechanism, by decreasing the efficiency of start codon recognition for the *ATG13* uORF compared to that for the *ATG13* CDS. Similarly, the uORFs for *ATG5, ATG12* and *ATG19*

have weak Kozak sequences or completely lack a canonical sequence, in line with a leaky-scanning mechanism. At present, we cannot make a definitive conclusion as to which mechanism, leaky scanning or translation reinitiation, is used in the context of the *ATG* uORFs, but overall our results favor the former.

We showed that uORF-mediated Atg13 translation is dependent on Gcn2 kinase activity in yeast. It has been reported that many human genes, such as *ATF4* and *ATF5*, exploit uORFs to regulate translation by EIF2 phosphorylation [22,54]. In human cells, there are four EIF2A/eIF2α kinases (EIF2AK1/HRI, EIF2AK2/PKR, EIF2AK3/PERK, and EIF2AK4/GCN2) involved in the integrated stress response [55]. These kinases are activated in response to various types of stress. Among all the human EIF2A kinases, EIF2AK4/GCN2 and EIF2AK3/PERK are altered upon nutrient deprivation and ER stress, respectively. uORFs regulate ATF4 translation in response to EIF2 phosphorylation during ER

stress. Because the upregulation of the ATG proteins with the omission of the uORFs seem to be most consistent with the translational control of Gcn4 in yeast or ATF4 in human, we think it is also possible and worth investigating whether activation of EIF2AK3/PERK by ER stress may have a potential role in uORF-mediated translational control of *ATG* genes in human cells.

We identified inhibitory effects of canonical uORFs on downstream CDS translation of *ATG5, ATG12, ATG13* and *ATG19* during both nutrient-replete and -depleted conditions; however, we are aware that the underlying translation regulation mechanism might be at least in part different from what we propose here. For example, the protein levels of Atg13 and Atg19 are both upregulated upon starvation. We did not observe a significant increase of Atg13 protein levels in the *ATG13* uORF mutant cells upon starvation compared to growing conditions, whereas in the *ATG19* uORF mutant cells, Atg19 protein levels were markedly enhanced upon starvation, suggesting that the identified *ATG19* uORF may have less impact on its CDS translation compared with the identified *ATG13* uORF. There are multiple possibilities to explain these observations. For example, *ATG19* mRNA may have more actively translated uORFs that were not identified by ribosome profiling due to the low sensitivity of translational signal capture, and thus the upregulation of the Atg19 protein by a starvation stimulus may not be fully eliminated by simply mutating one uORF. It is also possible that there exists a more dominant but currently unknown mechanism for Atg19 translational control, such as RNA-binding proteins and trans-acting regulators like microRNAs [56,57]. A previous study reported that Dhh1, a DExD/H-box RNA helicase, is required for efficient translation of some Atg proteins such as Atg1 and Atg13 [8]. RNA-binding proteins, such as ELAVL1, ELAVL4, HNRNPA1 and ZFP36, are involved in translation regulation of ATG5, ATG16, ATG7 and BECN1 in various human cell settings [10–14]. In addition, EIF5A is required for efficient ATG3 translation [58]. It will be interesting to further explore the mechanism by which some *ATG* genes regulate translation via a *cis*-acting uORF.

We also note that we observed that *ATG19* uORF mutant cells demonstrated a fold-change of 1.9 and 1.3 in Atg19-PA levels compared with WT cells in nutrient-rich and nitrogen-starvation conditions, respectively. However, an analysis of prApe1 maturation to monitor activity of the Cvt pathway did not show a difference between WT and *ATG19* uORF mutant cells (data not shown). Atg19 interacts with Atg11 prior to binding Atg8; thus, increasing the expression of Atg19 and not Atg11 may not be adequate to induce a significant change in the delivery of prApe1 to the vacuole via the Cvt pathway.

Mutations in either *ATG5* uORF1 or uORF2 resulted in enhanced total Atg5 and Atg12–Atg5 levels, as well as a consequent increase in autophagy. Intriguingly, although we observed a significant increase in these levels in cells containing mutations in *ATG5* uORF3 and uORF4, autophagy activity monitored by the GFP-Atg8 processing and Pho8Δ60 assays was not consequently enhanced. uORF3 encodes a dipeptide, and the stop codon of uORF3 and uORF4 is only 3 nucleotides upstream of the *ATG5* CDS. It is possible

that besides having a role in impeding the translation of the downstream CDS, the dipeptide generated by uORF3 is biologically functional and involved in autophagy activation. Due to technical limitations, we failed to directly overexpress or detect the uORF micro-peptide; however, a recent report showed that it is common that micro-peptides generated by uORFs are able to stabilize protein complexes together with CDS proteins [59]. Hence, the precise role of yeast *ATG5* uORF3 and uORF4 in autophagy regulation is yet to be uncovered. Furthermore, canonical uORFs are more conserved compared with non-canonical ones in general [25]. Therefore, it would be interesting to determine whether canonical uORFs of human *ATG5* display similar unknown features as the uORF3 of yeast *ATG5*.

A previous study showed that the translational enhancement of ATG5, ATG12 and ATG16L1 upon starvation is mediated by the interaction between the RNA binding protein ELAVL1/HuA and the 3' UTR of the corresponding mRNAs in human cells [60]. In addition, three canonical uORFs and many non-canonical uORFs of *ATG5* are predicted to be translationally active in human cells in our study, suggesting a very complex mechanism underlying ATG5 translation regulation and consequent autophagy induction upon stress. The detailed landscape requires further investigation.

Many studies indicated that gain and loss of uORFs frequently occur in the human population [15,61]. A subset of EIF2A-targeted uORFs regulate oncogenic mRNAs during early stages of tumorigenesis [62]. In addition to the scanning singleton variants associated with uORFs on *ATG* genes from the ExAc catalog (Figure 5), we also investigated if there are recurrent somatic mutations in cancers (obtained from the COSMIC database) occurring on predicted active uORFs of *ATG* genes in human [25,63]. Although 15 uORFs of *ATG* genes are linked with singleton variants in the ExAc catalog, we did not find any mutations in uORFs of *ATG* genes associated with cancers from COSMIC. The identification of uORFs of *ATG* genes affected by singleton variants from the ExAC catalog suggests that these uORFs play an essential role in regulating autophagy as it reflects considerable selection pressure. We were not surprised to find that no uORFs of *ATG* genes are recurrently associated with cancers. Although autophagy is broadly recognized to play a bidirectional role in tumor suppression and cancer cell growth promotion, mutations of core *ATG* genes in cancer are not common [64]. The escape of genetic mutations in uORFs of *ATG* genes is consistent with this phenomenon; this escape presumably occurs because proper autophagy is essential for maintaining nuclear and mitochondrial stability [3]. In addition, uORF mutations may cause excessive autophagy that are harmful for cell survival.

In summary, we found that canonical uORFs on the mRNA transcripts of multiple yeast *ATG* genes, including *ATG5, ATG12, ATG13*, and *ATG19*, inhibit downstream CDS translation under nutrient-rich conditions. The bypass of these uORFs plays an essential role in the translational upregulation of these *ATG* genes upon nitrogen starvation. *ATG13* uORF translation is largely dependent on its Kozak sequence as well as Gcn2 kinase activity. We showed that the defined *ATG5* uORF1 and uORF2 are essential for Atg5

translational control to regulate autophagy activation. Furthermore, we elucidated that non-canonical uORFs of human *ATG4B* and *ATG12* play an inhibitory role of downstream CDS translation by reducing translation efficiency. Functional activity of uORFs has been demonstrated for only a limited number of genes, such as *GCN4* in yeast and *ATF4* in human; we extended the examples to *ATG* genes, the genes encoding components of autophagy, a critical mechanism for cells to maintain survival and promote bioenergetic homeostasis in response to stress. Furthermore, there are currently no reports associating uORFs with the translational control of *ATG* genes. Thus, for the first time, we showed that a large subset of *ATG* genes is regulated by a specific uORF-mediated translational mechanism to modulate autophagy activity.

Materials and Methods

Yeast strains, media and growth conditions

Yeast strains used in this paper are listed in Table S4. For nutrient-rich conditions, yeast cells were grown in YPD medium (1% [wt:vol] yeast extract, 2% [wt:vol] peptone, 2% [wt:vol] glucose). Autophagy was induced by shifting mid-log phase yeast cells from rich medium to nitrogen-starvation medium SD-N (0.17% yeast nitrogen base without ammonium sulfate or amino acids, 2% [wt:vol] glucose) for the indicated times.

Key Reagents
Key Reagents used in the study are listed in Table 1.

Cell culture and HBSS starvation

The 293 FT (R70007) and HeLa (CCL-2) cell lines were obtained from Thermo Fisher Scientific and the American Type Culture Collection, respectively. These cells were cultured in Dulbecco's Modified Eagle's Medium (DMEM; Thermo Fisher Scientific, 11,995,073) supplemented with 10% heat-inactivated fetal bovine serum (Thermo Fisher Scientific, A3840001) and 1% penicillin and streptomycin (Thermo Fisher Scientific, 15,070–063) at 37°C, 95% humidity, and 5% CO_2. Hanks' balanced salt solution (HBSS) was obtained from Sigma-Aldrich (55037C). Starvation was induced by changing the DMEM medium to HBSS for 4 h. Cell line identity was validated by short tandem repeat profiling, and routine mycoplasma testing was negative for contamination.

Luciferase reporter assay

293 FT cells were seeded at a density of 5×10^4 cells per well in a 24-well plate and grown to 50% confluency. One μg of the 5' UTR-Firefly luciferase reporter construct (Addgene, 45968; deposited by Dr. Ralf Kuehn) and 100 ng of Renilla luciferase reporter construct (Addgene, 27163; deposited by Dr. Ron Prywes) were transfected into 293 FT cells using Lipofectamine 3000 (Invitrogen, L3000001). After 24 h, cells were treated with HBSS for an additional 4 h, and then Firefly and Renilla luciferase activities were determined using a Dual Luciferase Assay

System (Promega, E1910). Firefly luciferase signals were normalized to Renilla luciferase internal control signals in each experiment.

RT-qPCR

For yeast, the cells were cultured in YPD medium to mid-log phase, and an aliquot was collected as the nutrient-rich sample. The remaining cells were shifted to SD-N medium for autophagy induction. Cells were then collected and frozen in liquid nitrogen. Total RNA was extracted using an RNA extraction kit (NucleoSpin RNA II; Clontech, 740955.50). Reverse transcription was carried out using the High-Capacity cDNA Reverse Transcription Kit (Applied Biosystems/ThermoFisher Scientific, ILT4368814). RT-qPCR was performed using the Power SYBR Green PCR Master Mix (Applied Biosystems/ThermoFisher Scientific, ILT4367659). The relative abundance of reference mRNAs and normalization for different total RNA amounts was done as described previously [65,66].

For human cells, 293 FT cells were seeded at a density of 5×10^4 cells per well in a 24-well plate and grown to 50% confluency. One μg of the 5'UTR-Firefly luciferase reporter construct and 100 ng of Renilla luciferase reporter construct [67] were transfected into 293 FT cells using Lipofectamine 3000. After 24 h, cells were treated with HBSS for an additional 4 h. mRNA levels were determined by real-time PCR analysis.

Western blot

Western blot was performed as described previously [8,68]. The antiserum to Pgk1 was generously provided by Dr. Jeremy Thorner (University of California, Berkeley). Antibody to YFP (Clontech, 632381) was used to detect GFP-tagged proteins. Atg13-PA, Atg5-PA, Atg12-PA, and Atg19-PA were detected with antibody to PA (Jackson ImmunoResearch, 323–005-024). The endogenous antibody to Atg1 was described previously [69]. Western blot bands were quantified by Bio-Rad Image Lab Software. Lanes/bands were manually selected and added for lane file analysis. An analysis table showing band intensities was used to calculate relative protein expression levels. The bands used are described in the figure legends.

Plasmids

Plasmids used in the yeast cells were generated as follows: The *pRS406-ATG13 5'UTR-ATG13-PA* plasmid was made by fast-cloning from the integrating vector *pRS406* as described previously [8]. The DNA fragment containing 600 base pairs (bps) upstream of the start codon of *ATG13*, the ORF encoding ATG13-PA, and 423 bps downstream of the *ATG13* CDS was amplified by PCR from the genomic DNA of a yeast strain in which the *ATG13* gene was C-terminally-tagged with one copy of PA followed by the *ATG13* endogenous 3' UTR. *pRS406-ATG13 5'UTR^{mut}-ATG13-PA*, the plasmid with the *ATG13* uORF mutation, was generated by site-directed mutagenesis based on the *pRS406-ATG13 5'UTR-ATG13-PA* plasmid. Similarly, the *pRS406-ATG12 5'UTR-ATG12-PA* and *pRS406-ATG19 5'UTR-ATG19-PA* plasmids were generated by fast-cloning from the *pRS406* vector. The plasmids with uORF

Table 1. Key reagents used in these studies.

REAGENT or RESOURCE	SOURCE	IDENTIFIER
Antibodies		
Anti-YFP	Clontech	632381; RRID: AB_2313808
Anti-peroxidase (anti-protein A)	Jackson ImmunoResearch	323–005-024; RRID:AB_2315781
Anti-Pgk1	Dr. Jeremy Thorner	N/A
Anti-Atg1	In house	N/A
Goat anti-rabbit IgG, HRP	Fisher Scientific	ICN55676; RRID:AB_2334589
Rabbit anti-mouse IgG, HRP	Jackson ImmunoResearch	315–035-003; RRID:AB_2340061
Chemicals, peptides, and recombinant proteins		
Power SYBR Green PCR Master Mix	Applied Biosystems/ThermoFisher Scientific	ILT4367659
p-Nitrophenyl phosphate	Sigma-Aldrich	N4645
Complete EDTA-free protease inhibitor cocktail	Roche	05056489001
TURBO DNA-free kit	Fisher Scientific	AM1907
RNasin® PLUS Rnase inhibitor	Fisher Scientific	PRN2615
Lipofectamine 3000	Invitrogen	L3000001
Critical commercial assays		
BCA Protein assay	Fisher Scientific	PI23223, PI23224
Dual Luciferase Assay System	Promega	E1910
NucleoSpin® RNA II	Clontech	740955.50
High-Capacity cDNA Reverse Transcription Kit	Applied Biosystems/ThermoFisher Scientific	ILT4368814
DNA Gel Purification Kit	Qiagen	28706X4
Q5® Site-Directed Mutagenesis Kit	New England BioLabs	E0554S
Experimental models: Cell lines		
Human: HEK293-FT	Thermo Fisher Scientific	R70007
Human: HeLa	American Type Culture Collection	CCL-2
Experimental models: Organisms/strains		
S. cerevisiae: strain background: SEY6210	See Table S4	N/A
Oligonucleotides		
Primers for RT-qPCR in yeast	[66]	N/A
Primers for RT-qPCR in human	See Table S5	N/A
Primers for plasmid cloning and strains construction	See Table S6	N/A
Recombinant DNA		
pRS406-ATG13 5'UTR-ATG13-PA	This study	N/A
pRS406-ATG135'UTR^{mut}-ATG13-PA	This study	N/A
pRS406-ATG12 5'UTR-ATG12-PA	This study	N/A
pRS406-ATG125'UTR^{mut}-ATG12-PA	This study	N/A
pRS406-ATG19 5' UTR-ATG19-PA	This study	N/A
pRS406-ATG195'UTR^{mut}-ATG19-PA	This study	N/A
pRS416-ATG5 5'UTR-ATG5-PA	This study	N/A
pRS416-ATG55'UTR^{mut1}-ATG5-PA	This study	N/A
pRS416-ATG55'UTR^{mut2}-ATG5-PA	This study	N/A
pRS416-ATG55'UTR^{mut3}-ATG5-PA	This study	N/A
pCMV-ATG4B 5'UTR-LUC	This study	N/A
pCMV-ATG4B5'UTR^{mut}-LUC	This study	N/A
pCMV-ATG12 5'UTR-LUC	This study	N/A
pCMV-ATG125'UTR^{mut1}-LUC	This study	N/A
pCMV-ATG125'UTR^{mut2}-LUC	This study	N/A
pCMV-ATG125'UTR^{mut3}-LUC	This study	N/A
pCMV-ATG125'UTR^{mut4}-LUC	This study	N/A
pRL-SV40P	[67]	Addgene, 27163; deposited by Ron Prywes
Software and algorithms		
CFX Manager Software	Bio-Rad	N/A
R studio	R studio®	https://www.rstudio.com/
Bio-Rad Image Lab Software	Bio-Rad	
GraphPad Prism 9	GraphPad	https://www.graphpad.com/

mutations, *pRS406-ATG19 5'UTR^{mut}-ATG19-PA* and *pRS406-ATG12 5'UTR^{mut}-ATG12-PA* were mutated by site-directed mutagenesis. These integrating plasmids were linearized using StuI before being integrated into the corresponding strains. The *pRS416-ATG5 5'UTR-ATG5-PA* plasmid was generated by fast-cloning from the centromeric vector pRS416. uORF mutation versions of the *pRS416-ATG5 5'UTR-ATG5-PA* plasmid, including *pRS416-ATG5 5'UTR^{mut1}-ATG5-PA*, *pRS416-ATG5 5'UTR^{mut2}-ATG5-PA*, and *pRS416-ATG5 5'UTR^{mut3}-ATG5-PA* were generated by site-directed mutagenesis.

Plasmids used in the human cells were generated as follows: 518 nucleotides of the 5' UTR of *ATG4B* mRNA and 315 nucleotides of the 5' UTR of *ATG12* mRNA containing the wild-type uORFs were PCR-amplified using DNA polymerase on genomic DNA derived from the HeLa cell line, together with PCR primers. PCR-amplified 5' UTRs were purified using a DNA Gel Purification Kit (Qiagen, 28706X4), digested with *Kpn*I and *Mlu*I, and inserted into the *Kpn*I and *Mlu*I sites of a Firefly luciferase reporter system using T4 DNA ligase (New England BioLabs, M0202S). Site directed mutagenesis of uORFs were performed using a kit (New England BioLabs,

E0554S) with PCR primers. The sequence of constructs was confirmed by dideoxy sequencing.

Identification of putative uORFs of ATG genes

The following published datasets were analyzed in this study: (1) All possible canonical uORFs annotated by ribosome profiling performed by Ingolia et al. [17]; (2) canonical and noncanonical uORFs catalog predicted by a machine learning algorithm from the study by McGillivray et al. [25]. Potential translational active uORFs associated with core *ATG* genes were extracted and further analyzed based on their position, type, and start codon usage, etc. as shown in Tables S1 and S2.

Autophagy assays

The Pho8Δ60 assay and GFP-Atg8 processing assay were performed as described previously [29,70].

Statistical Analysis

Statistical analyses were performed using GraphPad Prism 9. Statistical significance was determined from at least 3 independent experiments using either Student's *t*-test or ANOVA. *: $p < 0.05$; **: $p < 0.01$; ***: $p < 0.005$. Number of independent experiments (n), statistical test utilized, dispersion of measurements and significance are described in the figure legends.

Disclosure statement

The authors declare no competing interests.

ORCID

Ying Yang 🔟 http://orcid.org/0000-0003-1602-1212
Rui Kang 🔟 http://orcid.org/0000-0003-2725-1574
Daolin Tang 🔟 http://orcid.org/0000-0002-1903-6180
Daniel J. Klionsky 🔟 http://orcid.org/0000-0002-7828-8118

References

[1] Yin Z, Popelka H, Lei Y, et al. The Roles of Ubiquitin in Mediating Autophagy. Cells. 2020;9(9):2025. DOI:10.3390/cells9092025.

[2] Wen X, Yang Y, Klionsky DJ. Moments in autophagy and disease: past and present. Mol Aspects Med. 2021 April 28;82:100966.10.1016/j.mam.2021.100966

[3] Yang Y, Klionsky DJ. Autophagy and disease: unanswered questions.Cell Death Differ. 2020 [2020 March 01];27(3):858–871.DOI:10.1038/s41418-019-0480-9.

[4] Parzych KR, Ariosa A, Mari M, et al. A newly characterized vacuolar serine carboxypeptidase, Atg42/Ybr139w, is required for normal vacuole function and the terminal steps of autophagy in the yeast Saccharomyces cerevisiae. Mol Biol Cell. 2018;29(9):1089–1099. DOI:10.1091/mbc.E17-08-0516.

[5] Feng Y, Yao Z, Klionsky DJ. How to control self-digestion: transcriptional, post-transcriptional, and post-translational regulation of autophagy.Trends Cell Biol. 2015 [2015 June 01];25(6):354–363. DOI:10.1016/j.tcb.2015.02.002.

[6] Chikashige Y, Kato H, Thornton M, et al. Gcn2 eIF2α kinase mediates combinatorial translational regulation through nucleotide motifs and uORFs in target mRNAs. Nucleic Acids Res. 2020;48(16):8977–8992. DOI:10.1093/nar/gkaa608.

[7] Zou K, Ouyang Q, Li H, et al. A global characterization of the translational and transcriptional programs induced by methionine restriction through ribosome profiling and RNA-seq. BMC Genomics. 2017 February 17 18(1):189. 10.1186/s12864-017-3483-2

[8] Liu X, Yao Z, Jin M, et al. Dhh1 promotes autophagy-related protein translation during nitrogen starvation. PLoS Biol. 2019;17(4):e3000219. DOI:10.1371/journal.pbio.3000219.

[9] Yin Z, Liu X, Ariosa A, et al. Psp2, a novel regulator of autophagy that promotes autophagy-related protein translation. Cell Res. 2019 December 01 29(12):994–1008. 10.1038/s41422-019-0246-4

[10] Acevo-Rodríguez PS, Maldonado G, Castro-Obregón S, et al. Autophagy regulation by the translation machinery and its implications in cancer [Review]. Front Oncol. 2020 March 13;10(322). DOI:10.3389/fonc.2020.00322.

[11] Kim C, Kim W, Lee H, et al. The RNA-binding protein HuD regulates autophagosome formation in pancreatic β cells by promoting autophagy-related gene 5 expression. J Biol Chem. 2014;289(1):112–121. DOI:10.1074/jbc.M113.474700.

[12] Ji E, Kim C, Kang H, et al. RNA binding protein HuR promotes autophagosome formation by regulating expression of autophagy-related proteins 5, 12, and 16 in human hepatocellular carcinoma cells. Mol Cell Biol. 2019;39(6):e00508–18. DOI:10.1128/MCB.00508-18.

[13] Palanisamy K, Tsai TH, Yu TM, et al. RNA-binding protein, human antigen R regulates hypoxia-induced autophagy by targeting ATG7/ATG16L1 expressions and autophagosome formation. J Cell Physiol. 2019;234(5):7448–7458. DOI:10.1002/jcp.27502.

[14] Zhang Z, Guo M, Li Y, et al. RNA-binding protein ZFP36/TTP protects against ferroptosis by regulating autophagy signaling pathway in hepatic stellate cells. Autophagy. 2020;16(8):1482–1505. DOI:10.1080/15548627.2019.1687985.

[15] Calvo SE, Pagliarini DJ, Mootha VK. Upstream open reading frames cause widespread reduction of protein expression and are polymorphic among humans. Proceedings of the National Academy of Sciences. 2009;106(18):7507–7512.

[16] Zhang H, Wang Y, Lu J. Function and evolution of upstream ORFs in eukaryotes. Trends Biochem Sci. 2019;44(9):782–794.

[17] Ingolia NT, Ghaemmaghami S, Newman JRS, et al. Genome-wide analysis in vivo of translation with nucleotide resolution using ribosome profiling. Science. 2009;324(5924):218–223. DOI:10.1126/science.1168978.

[18] Fernandez J, Yaman I, Huang C, et al. Ribosome stalling regulates IRES-mediated translation in eukaryotes, a parallel to prokaryotic attenuation. Mol Cell. 2005 [2005 February 04];17(3):405–416. DOI:10.1016/j.molcel.2004.12.024.

[19] Hinnebusch AG. Translational regulation of GCN4 and the general amino acid control of yeast. Annu Rev Microbiol. 2005;59:407–450.

[20] Munzarová V, Pánek J, Gunišová S, et al. Translation Reinitiation Relies on the Interaction between eIF3a/TIF32 and Progressively Folded cis-Acting mRNA Elements Preceding Short uORFs. PLoS Genet. 2011;7(7):e1002137. DOI:10.1371/journal.pgen.1002137.

[21] Andrews SJ, Rothnagel JA. Emerging evidence for functional peptides encoded by short open reading frames.Nat Rev Genet. 2014 [2014 March 01];15(3):193–204.DOI:10.1038/nrg3520.

[22] Vattem KM, Wek RC. Reinitiation involving upstream ORFs regulates ATF4 mRNA translation in mammalian cells. Proceedings of the National Academy of Sciences of the United States of America. 2004;101(31):11269–11274.

[23] Ingolia NT, Brar GA, Rouskin S, et al. The ribosome profiling strategy for monitoring translation in vivo by deep sequencing of ribosome-protected mRNA fragments. Nat Protoc. 2012 August 01 7(8):1534–1550. 10.1038/nprot.2012.086

[24] Chew G-L, Pauli A, Schier AF. Conservation of uORF repressiveness and sequence features in mouse, human and zebrafish.Nat Commun. 2016 [2016 May 24];7(1):11663.DOI:10.1038/ncomms11663.

[25] McGillivray P, Ault R, Pawashe M, et al. A comprehensive catalog of predicted functional upstream open reading frames in humans. Nucleic Acids Res. 2018;46(7):3326–3338. DOI:10.1093/nar/gky188.

[26] Reggiori F, Tucker KA, Stromhaug PE, et al. The Atg1-Atg13 complex regulates Atg9 and Atg23 retrieval transport from the pre-autophagosomal structure. Dev Cell. 2004 Jan;6(1):79–90. DOI:10.1016/S1534-5807(03)00402-7.

[27] Klionsky DJ, Abdel-Aziz AK, Abdelfatah S, et al. Guidelines for the use and interpretation of assays for monitoring autophagy (4th edition)1. Autophagy. [2021 January 02];17(1):1–382.

[28] Cheong H, Klionsky DJ. Biochemical methods to monitor autophagy-related processes in yeast. Methods Enzymol. 2008;451:1–26.

[29] Memisoglu G, Eapen VV, Yang Y, et al. PP2C phosphatases promote autophagy by dephosphorylation of the Atg1 complex. Proceedings of the National Academy of Sciences. 2019:201817078.

[30] Hinnebusch AG, Ivanov IP, Sonenberg N. Translational control by 5'-untranslated regions of eukaryotic mRNAs. Science. 2016 Jun 17; 352(6292):1413–1416. 10.1126/science.aad9868

[31] Sonenberg N, Hinnebusch AG. Regulation of translation initiation in eukaryotes: mechanisms and biological targets. Cell. 2009 Feb 20; 136(4):731–745. 10.1016/j.cell.2009.01.042

[32] Kozak M. Point mutations define a sequence flanking the AUG initiator codon that modulates translation by eukaryotic ribosomes. Cell. 1986 Jan 31; 44(2):283–292. 10.1016/0092-8674(86)90762-2

[33] Barbosa C, Peixeiro I, Romão L. Gene expression regulation by upstream open reading frames and human disease. PLoS Genet. 2013;9(8):e1003529.

[34] Kim M, Sandford E, Gatica D, et al. Mutation in ATG5 reduces autophagy and leads to ataxia with developmental delay. Elife. 2016 Jan 26;5: 10.7554/eLife.12245

[35] Mizushima N, Noda T, Yoshimori T, et al. A protein conjugation system essential for autophagy. Nature. 1998 September 1 395 (6700):395–398. 10.1038/26506

[36] Walczak M, Martens S. Dissecting the role of the Atg12-Atg5-Atg16 complex during autophagosome formation. Autophagy. 2013 Mar;9(3):424–425.

[37] Hanada T, Noda NN, Satomi Y, et al. The Atg12-Atg5 Conjugate Has a Novel E3-like Activity for Protein Lipidation in Autophagy*. J Biol Chem. 2007 December 28 282 (52):37298–37302. 10.1074/jbc.C700195200

[38] Scott SV, Guan J, Hutchins MU, et al. Cvt19 is a receptor for the cytoplasm-to-vacuole targeting pathway. Mol Cell. 2001 Jun;7(6):1131–1141.DOI:10.1016/S1097-2765(01)00263-5.

[39] Andreev DE, Arnold M, Kiniry SJ, et al. TASEP modelling provides a parsimonious explanation for the ability of a single uORF to derepress translation during the integrated stress response. Elife. 2018;7:e32563.

[40] Fritsch C, Herrmann A, Nothnagel M, et al. Genome-wide search for novel human uORFs and N-terminal protein extensions using ribosomal footprinting. Genome Res. 2012;22(11):2208–2218. DOI:10.1101/gr.139568.112.

[41] Lee S, Liu B, Lee S, et al. Global mapping of translation initiation sites in mammalian cells at single-nucleotide resolution. Proceedings of the National Academy of Sciences. 2012;109(37):E2424–E2432.

[42] Feng Y, He D, Yao Z, et al. The machinery of macroautophagy. Cell Res. 2014 January 1 24(1):24–41. 10.1038/cr.2013.168

[43] Kearse MG, Wilusz JE. Non-AUG translation: a new start for protein synthesis in eukaryotes. Genes Dev. 2017;31 (17):1717–1731.

[44] Spealman P, Naik AW, May GE, et al. Conserved non-AUG uORFs revealed by a novel regression analysis of ribosome profiling data. Genome Res. 2018 Feb;28(2):214–222.DOI:10.1101/gr.221507.117.

[45] Tennessen JA, Bigham AW, O'Connor TD, et al. Evolution and functional impact of rare coding variation from deep sequencing of human exomes. Science. 2012;337(6090):64–69. DOI:10.1126/science.1219240.

[46] Lek M, Karczewski KJ, Minikel EV, et al. Analysis of protein-coding genetic variation in 60,706 humans. Nature. 2016 July 1 536(7616):285–291. 10.1038/nature19057

[47] Ke X, Taylor MS, Cardon LR. Singleton SNPs in the human genome and implications for genome-wide association studies. Eur J Hum Genet. 2008 March 1; 16(4):506–515. 10.1038/sj.ejhg.5201987

[48] Li M, Hou Y, Wang J, et al. Kinetics comparisons of mammalian Atg4 homologues indicate selective preferences toward diverse Atg8 substrates. J Biol Chem. 2011 Mar 4 286(9):7327–7338. 10.1074/jbc.M110.199059

[49] Michel AM, Andreev DE, Baranov PV. Computational approach for calculating the probability of eukaryotic translation initiation from ribo-seq data that takes into account leaky scanning. BMC Bioinformatics. 2014 November 21; 15(1):380. 10.1186/s12859-014-0380-4

[50] Noda NN, Fujioka Y, Hanada T, et al. Structure of the Atg12–Atg5 conjugate reveals a platform for stimulating Atg8–PE conjugation. EMBO Rep. 2013;14(2):206–211. DOI:10.1038/embor.2012.208.

[51] Otomo C, Metlagel Z, Takaesu G, et al. Structure of the human ATG12~ATG5 conjugate required for LC3 lipidation in autophagy. Nat Struct Mol Biol. 2013 January 1 20(1):59–66. 10.1038/nsmb.2431

[52] Xia X, Dermitzakis E. The +4G site in kozak consensus is not related to the efficiency of translation initiation. PLOS ONE. 2007;2(2):e188.

[53] Kozak M. Effects of intercistronic length on the efficiency of reinitiation by eucaryotic ribosomes. Mol Cell Biol. 1987;7 (10):3438–3445.

[54] Watatani Y, Ichikawa K, Nakanishi N, et al. Stress-induced translation of ATF5 mRNA is regulated by the 5'-untranslated region. J Biol Chem. 2008 Feb 1 283(5):2543–2553. 10.1074/jbc.M707781200

[55] Andreev DE, O'Connor PB, Fahey C, et al. Translation of 5' leaders is pervasive in genes resistant to eIF2 repression. Elife. 2015 Jan 26;4:e03971.10.7554/eLife.03971.

[56] Babitzke P, Baker CS, Romeo T. Regulation of translation initiation by RNA binding proteins. Annu Rev Microbiol. 2009;63:27–44.

[57] Cottrell KA, Szczesny P, Djuranovic S. Translation efficiency is a determinant of the magnitude of miRNA-mediated repression. Sci Rep. 2017 November 02; 7(1):14884. 10.1038/s41598-017-13851-w

[58] Lubas M, Harder LM, Kumsta C, et al. eIF5A is required for autophagy by mediating ATG3 translation. EMBO Rep. 2018 Jun;19(6). doi:10.15252/embr.201846072.

[59] Chen J, Brunner A-D, Cogan JZ, et al. Pervasive functional translation of noncanonical human open reading frames. Science. 2020;367(6482):1140–1146. DOI:10.1126/science.aay0262.

[60] Ji E, Kim C, Kang H, et al. RNA binding protein hur promotes autophagosome formation by regulating expression of

autophagy-related proteins 5, 12, and 16 in human hepatocellular carcinoma cells. mol cell biol. 2019 mar 15;39:(6):e00508–18.

[61] Zhang H, Dou S, He F, et al. Genome-wide maps of ribosomal occupancy provide insights into adaptive evolution and regulatory roles of uORFs during Drosophila development. PLoS Biol. 2018;16(7):e2003903. DOI:10.1371/journal.pbio.2003903.

[62] Sendoel A, Dunn JG, Rodriguez EH, et al. Translation from unconventional 5' start sites drives tumour initiation. Nature. 2017;541(7638):494–499. DOI:10.1038/nature21036.

[63] Forbes SA, Beare D, Boutselakis H, et al. COSMIC: somatic cancer genetics at high-resolution. Nucleic Acids Res. 2016;45(D1):D777–D783. DOI:10.1093/nar/gkw1121.

[64] Amaravadi R, Kimmelman AC, White E. Recent insights into the function of autophagy in cancer. Genes Dev. 2016 Sep 1; 30 (17):1913–1930. 10.1101/gad.287524.116

[65] Gatica D, Hu G, Liu X, et al. The Pat1-Lsm complex stabilizes ATG mRNA during nitrogen starvation-induced autophagy. Mol Cell. 2019 January 17 73(2):314–324.e4. 10.1016/j.molcel.2018.11.002

[66] Hu G, McQuiston T, Bernard A, et al. A conserved mechanism of TOR-dependent RCK-mediated mRNA degradation regulates autophagy. Nat Cell Biol. 2015 July 1 17(7):930–942. 10.1038/ncb3189

[67] Chen X, Prywes R. Serum-induced expression of the cdc25A gene by relief of E2F-mediated repression. Mol Cell Biol. 1999 Jul;19 (7):4695–4702.

[68] Feng Y, Ariosa AR, Yang Y, et al. Downregulation of autophagy by Met30-mediated Atg9 ubiquitination. Proceedings of the National Academy of Sciences. 2021;118(1):e2005539118.

[69] Abeliovich H, Zhang C, William A, et al. Chemical genetic analysis of apg1 reveals a non-kinase role in the induction of autophagy. Mol Biol Cell. 2003;14(2):477–490. DOI:10.1091/mbc.e02-07-0413.

[70] Feng Y, Backues SK, Baba M, et al. Phosphorylation of Atg9 regulates movement to the phagophore assembly site and the rate of autophagosome formation. Autophagy. 2016 April 2 12 (4):648–658. 10.1080/15548627.2016.1157237